THE ELECTRICAL CONDUCTIVITY OF THE MOON

L.L. VANYAN
Soviet Geophysical Committee, Moscow II7296, U.S.S.R.

Abstract. Investigations of the lunar electrical conductivity were described in excellent reviews by Sonett (1974) and Dyal *et al.* (1976). In this paper we will try to consider some new aspects of this problem in comparison with the Earth's data.

Basic Principles

As in the case of Earth induction, the EM-sounding of the Moon is based on Faraday's law. The main role in lunar excitation belongs to the TE-mode while the contribution of the TM-mode can be neglected due to very high resistivity of the near-surface dry lunar layer.

The Moon has neither a magnetosphere nor an ionosphere with current systems. The only sources of induction are electrical currents in interplanetary plasma, running past the Moon like plane waves. If the solar wind velocity is as great as 10^3 km/sec and magnetic fluctuations have periods about 10^2 sec, the wavelength reaches 10^5 km, i.e. some order to magnitude greater than the lunar radius. In this case one can consider this plane wave as a spatially homogeneous time harmonic magnetic field. Such a field can be described by the first spherical harmonic. However, if the solar wind velocity is only 150 km/sec and the period of fluctuations decreases to 10 sec, the wave lengths become shorter than the radius of the Moon. This corresponds approximately to the sixth-order spherical harmonic.

Note, that the greater the harmonic number, the smaller the thickness of the layer which we can investigate. The greatest depth (not more than half a radius) can be investigated by using the first harmonic. Therefore one must try to use actually the first harmonic for lunar sounding. Unfortunately there is an additional cause which provides high harmonics, namely, the asymmetry of the lunar environment.

Asymmetric Model of Electromagnetic Induction in the Moon

During each revolution around the Earth the Moon crosses three different regions (Figure 1).

(1) The Earth's magnetic tail, where very low plasma density is observed.

(2) Solar wind where plasma flows in the antisolar direction with the frozen-in magnetic field.

(3) The magnetosheath which is the outer shell of the magnetosphere. In this area

Geophysical Surveys **4** (1980) 173-185. 0046-5763/80/0041 – 0173$01.95

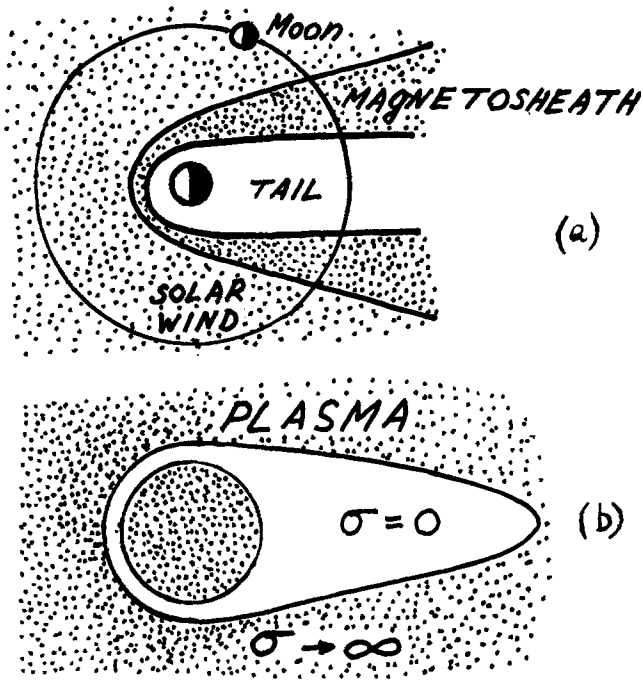

Fig. 1. (a) The Lunar orbit. (b) The Moon with cavity.

plasma density and magnetic fluctuations are enhanced.

Only in the first region is EM-induction in the Moon similar to that in the Earth. As to the solar wind and magnetosheath the role of the plasma is very significant here.

Note that the main volume of experimental data was obtained exactly in these regions.

Protons and electrons of the solar wind strike the day side of the Moon and are neutralized at the lunar surface. Therefore a shadow or lunar cavity is observed behind the Moon where there is no plasma. The length of the cavity is some lunar radii.

The magnetic field of the currents induced in the Moon propagates in the lunar cavity as in a vacuum, but is strongly damped in the surrounding plasma. Calculations show the skin-depth to be about 1–5 km. One can neglect this value and assume that at the plasma boundary the normal component of the induced field is zero as at a perfect conductor. Thus the total field, i.e. the sum of the external and induced parts, is equal simply to the corresponding component of the external magnetic fluctuation intensity. This is used as the boundary condition in the mathematical considerations.

The lunar cavity asymmetry, as was mentioned above, excites the high-order harmonics of the magnetic field. Only mathematical analysis gives us the possibility of determining favourable zones at the lunar surface where the contribution of these harmonics is the least.

Mathematical Description

A quasi-stationary EM-field in homogeneous conducting layers satisfies the diffusion equation.

It is convenient for theoretical investigations to transform all magnetic fields to the frequency domain and to use Helmholtz' equation. In the cavity and uppermost dielectric shell, Laplace's equation is satisfied. For the scalar magnetic potential in this area we have the well-known expansion:

$$U = \sum_{n=1}^{\infty} \sum_{m=0}^{n} (a_n^m R^n + b_n^m R^{-n-1}) S_n^m(\theta, \lambda). \tag{1}$$

At the plasma boundary $-(\partial U/\partial p) = B_p^e$, where p is the normal to the boundary. At the lower boundary of the dielectric shell the continuity of the potential and its radial derivative lead to the equation:

$$\frac{n a_n^m - (n+1) b_n^m r^{-2n-1}}{a_n^m + b_n^m} = -\frac{n(n+1)}{i\omega r} Z_n(\omega) \tag{2}$$

where $Z_n(\omega)$ is the impedance for the spherical harmonic with order n and angular frequency ω. Here r is the lower boundary of the dielectric shell.

The three- dimensional Laplace equation has been solved numerically (Egorov, 1978). Results of the calculations, some of which are shown in Figure 2, allow the following conclusions:

(1) Horizontal components of the magnetic variations at the lunar day side are several times greater than the external field. This is caused by the compression of magnetic field lines between the plasma and the inner conducting part of the Moon. The amplification of the magnetic field decreases with period.

(2) The magnetic field at the day-side has a slight dependence on the length of the lunar cavity. This dependence vanishes when the cavity is longer than three lunar radii. Note the solution of the induction problem in the Moon with an infinitely long cavity (Schwartz and Schubert, 1973).

(3) If the external field is parallel to the cavity axis, the first harmonic prevails over all the day side.

(4) If the external field is perpendicular to the cavity axis, there is a favourable area around the subsolar point where the first harmonic contribution is not less than 80%. The diameter of this area is about 80°.

(5) The horizontal magnetic field on the night side is 15 or 20% larger than for the sphere in vacuum.

(6) The radial component on the day-side yields no information on the conductivity distribution. On the night side this component decreases. The higher the frequency and

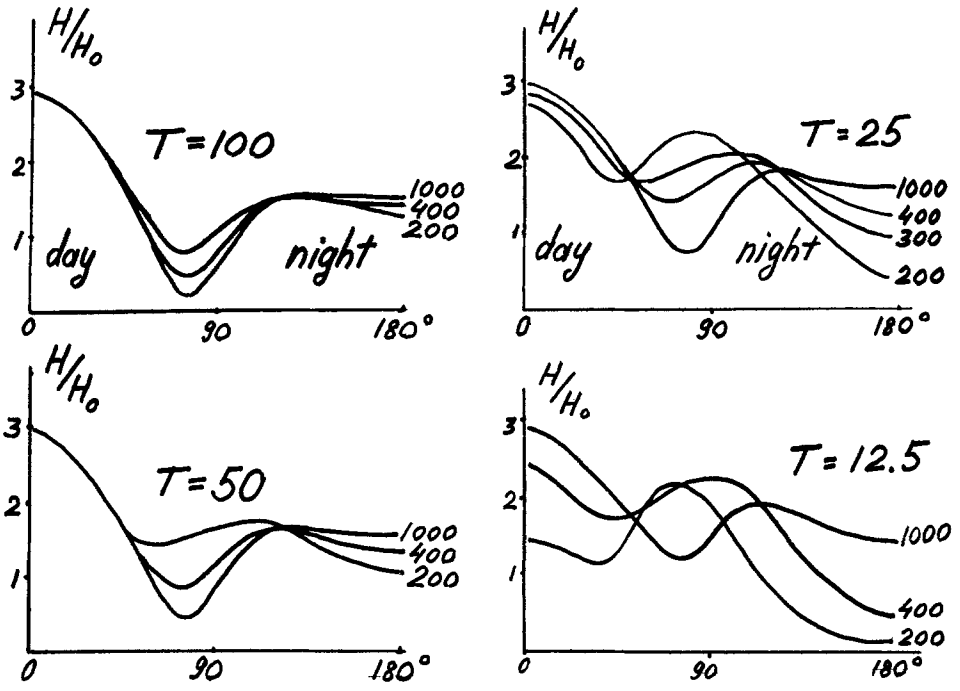

Fig. 2. The meridional magnetic component along the noon-midnight meridian at the lunar surface for different values of period T(sec). Curves are labelled by the solar wind velocity (km/sec). The thickness of the dielectric shell is 240 km and the resistivity of the inner part is 10^3 Ωm.

conductivity, the smaller the radial magnetic field. In general, the role of currents flowing at the cavity boundaries may be rather significant.

But, as for the day side, one can determine the favourable area around the antisolar point where the contribution of the boundary currents is less than 25%. The diameter of this area is about 60°.

Technique of the Magnetovariation Lunar Sounding

No measurement was made of the lunar electric variations which could be used for MT-sounding. The only way to estimate the lunar electrical conductivity is to interpret the magnetic response. This can be defined as the ratio of the horizontal or vertical variation intensity measured at one point on the surface to the parallel component, measured by the lunar satellite Explorer 35 (i.e. to the component of the external field).

If magnetic variations are observed in favourable zones at the lunar surface one can use two simplified models with spherical symmetry:

(1) The model for the day-side without a cavity behind the Moon.

(2) The model for the night-side without plasma around the Moon.

Lunar magnetic responses can be obtained both in the frequency and the time domain (the latter for the step-like pulse of the external field). The day-side frequency response $\tilde{h}_\tau$ decreases with period, whereas the night side response $\tilde{h}_r$ increases. The common low frequency limit for both responses is unity.

It is interesting to present the results of observations in a visual form. Vanyan and Egorov (1973) proposed the use of apparent resistivity for this purpose. This is possible because at short periods both day-side and night-side responses are connected with the Tikohonov–Cagniard impedance:

$$\tilde{h}_\tau \approx - \frac{i\omega\mu q}{Z}, \quad \tilde{h}_r \approx - \frac{3Z}{i\omega\mu q}$$

where Z is the impedance and q is the lunar radii. The apparent resistivity ρ_a can be obtained by the formulas:

$$\rho_a = \begin{cases} 5.98 \times 10^6 \, T^{-1} \, \tilde{h}_\tau^{-2} \, (\omega) & \text{for the frequency day-side response,} \\ 2.67 \times 10^6 \, T^{-1} \, \tilde{h}_r^{2} \, (\omega) & \text{for the frequency night-side response,} \\ 3.03 \times 10^5 \, t^{-1} \, \tilde{h}_\tau^{-2} \, (t) & \text{for the transient day-side response,} \\ 1.33 \times 10^5 \, t^{-1} \, \tilde{h}_r^{2} \, (\mathrm{t}) & \text{for the transient night-side response.} \end{cases}$$

Note, that ρ_a in the frequency domain is equal to the usual Tikhonov–Cagniard apparent resistivity.

The interesting possibility of lunar sounding using two surface magnetometers with no satellite data has recently been described by Vanyan *et al.* (1977).

Let us consider the new technique for determining the external field and applying it to synchronous Apollo 16 and Lunokhod 2 data. This model is adequate if the field measurement sites are situated far enough from the terminator to neglect the field asymmetry caused by the plasma cavity behind the Moon. As has been shown by Schubert *et al.* (1973) for an infinitely extended cavity, and by Vanyan and Egorov (1973) for a cavity of finite length, the assumption of a spherically symmetric model is valid over an angular range of 40° from the sub-solar point.

To develop this analysis with two surface measurements of the magnetic field, we consider a great circle on the lunar sphere through Apollo 16 and Lunokhod 2 surface sites (dashed line in Figure 3). To estimate the lunar response we utilize the horizontal component tangent to the great circle at the Apollo 16 site:

$$B_{\tau \mathrm{Ap}} = B_{z\mathrm{Ap}} \cos\phi + B_{y\mathrm{Ap}} \sin\phi \tag{3}$$

where ϕ is the angle between tangents to the great circle and the meridian intersecting at the Apollo 16 site; $B_{z\mathrm{Ap}}$ and $B_{y\mathrm{Ap}}$ are horizontal northward and eastward field

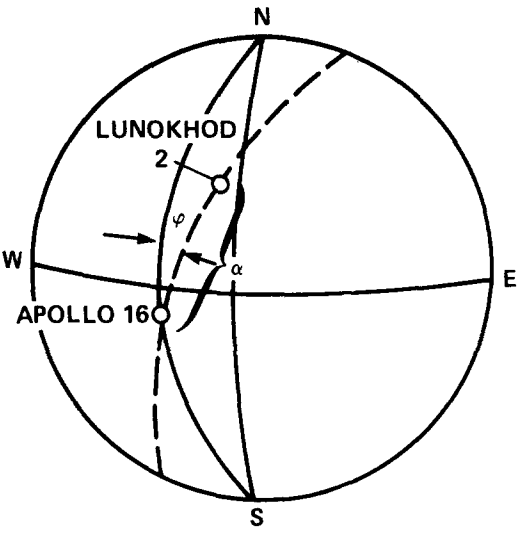

Fig. 3. Apollo 16 and Lunokhod 2 site locations on the day side of the Moon for February 13, 1973. The great circle connecting the sites is shown as a dashed line. ϕ is the azimuthal angle between the meridian passing through the Apollo 16 site and the great circle passing through both landing sites; α is the angle between radius vectors to the two magnetometer sites.

components, respectively. A determination of the external field compoent $B^e_{\tau \mathrm{Ap}}$ parallel to $B_{\tau \mathrm{Ap}}$ will allow us to complete a transient response calculation. $B^e_{\tau \mathrm{Ap}}$ can be determined from radial components $B_{r\mathrm{Ap}}$ and $B_{r\mathrm{L}}$ recorded synchronously by Apollo 16 and Lunokhod 2. We note that both these components lie in the plane of the great circle. From the equation which relates the Apollo 16 to the Lunokhod 2 coordinate systems in the plane of their common great circle we obtain:

$$B^e_\tau = B_{r\mathrm{L}} \operatorname{cosec} \alpha - B_{r\mathrm{Ap}} \cot \alpha$$

where $\alpha = 38^\circ$ is the angle between radius vectors to Apollo 16 and Lunokhod 2.

As an example to illustrate the new technique we consider the magnetic field discontinuity recorded at 17 h 12 m on February 13, 1973, when the Moon was in the magnetosheath. Figure 3 shows the dayside of the Moon on that date, and we note that both the Apollo 16 and Lunokhod 2 sites were situated far enough from the terminator at that time to neglect field confinement asymmetry effects. Lunokhod 2 was located in the southern part of le Monnier crater at the eastern boundary of Mare Serenitatis.

The Apollo 16 magnetometer is located at 8.9°S latitude 15.5°E longitude. Figure 4 shows plots of the radial components of the data, $B_{r\mathrm{Ap}}$ and $B_{r\mathrm{L}}$, at the two sites and the tangential component $B_{\tau \mathrm{Ap}}$ at the Apollo site calculated from Equation (3). The magnetic transient external to the Moon, B^e_τ plotted in Figure 4 was calculated using equation (4).

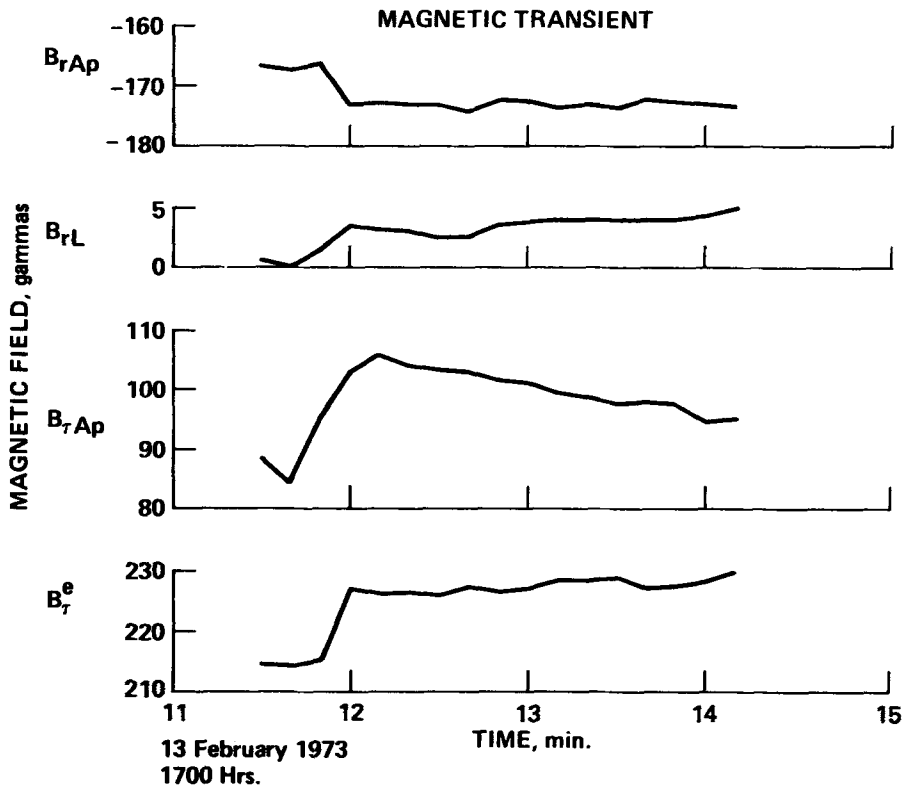

Fig. 4. Simultaneous Apollo 16 and Lunokhod 2 magnetograms from Frebruary 13, 1973. $B_{r\mathrm{Ap}}$ and $B_{r\mathrm{L}}$ are the radial components of measured magnetic fields at the Apollo 16 and Lunokhod 2 sites respectively. $B_{T\mathrm{Ap}}$ is the field component tangent to the lunar surface at the Apollo 16 site. B_T^e is the field component external to the Moon (calculated using $B_{r\mathrm{Ap}}$ and $B_{r\mathrm{L}}$) which corresponds to the measured total lunar response field $B_{T\mathrm{Ap}}$.

Statistical Data

Statistical data obtained at the time of the synchronized work of the magnetometers of Apollo 12 and Explorer 35 were published in the form of four independent characteristics. A group of investigators led by P. Dyal (Dyal *et al.*, 1974) obtained the daytime enhancements and night time diminutions in the time domain. Sonett *et al.* (1972) published data of similar characteristics of the response of the Moon to variations of the interplanetary magnetic field in the frequency domain.

It would be very desirable to combine these four characteristics into one. Such a combination has been carried out in the present paper in two steps. As the first step, the frequency characteristics of the transient responses were obtained by means of a numerical Fourier transform. The second step was to transform night-time diminutions into daytime enhancements by the equation $3/h_r - 1 = 2h_T$ (Vanyan and Egorov, 1973).

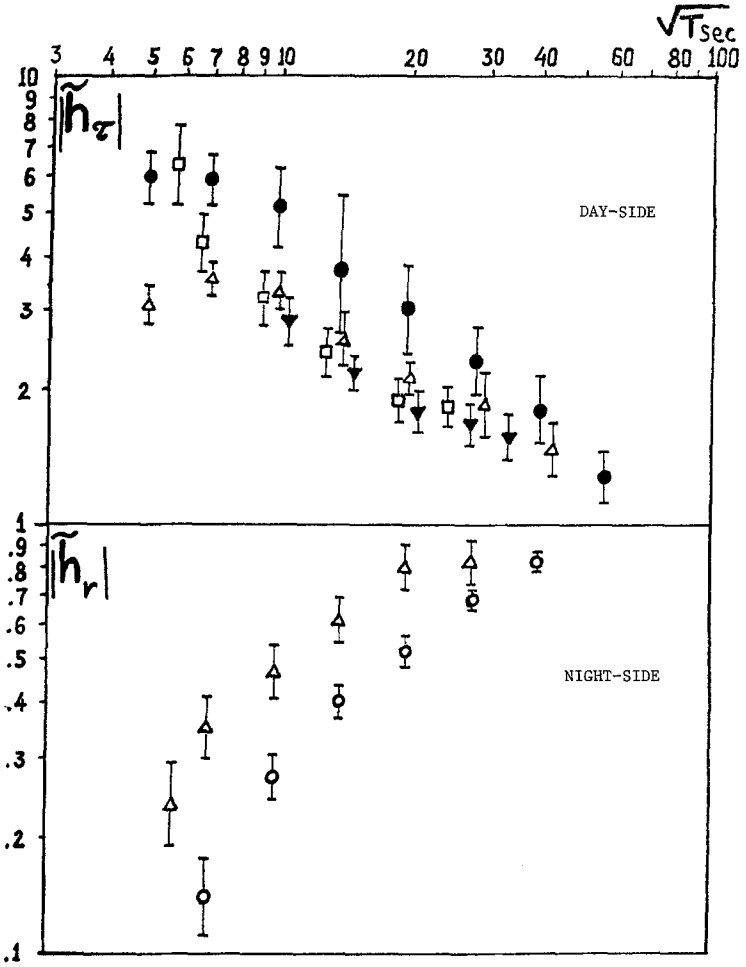

Fig. 5. Summarized data on the frequency response of the Moon obtained by Apollo 12 and 15: △,0-measurements of the day-side and night-side response (Sonett *et al.*, 1972); ● – Fourier transforms of transients observed by Dyal *et al.* (1974); □ – day-side response calculated from night-side one; ▼ – Apollo 15 data.

In this way a family of frequency characteristics for the daytime enhancements was found (Figure 5). A scatter between the different curves of the family served as a measure of the accuracy of the conductivity model of the Moon, since the velocity of propagation of interplanetary disturbances and the size of the plasma shadow affect the magnetic variations on the day- and night-time hemispheres quite differently in the frequency and time domains.

One can see that the intensity of horizontal magnetic variations on the lunar day side is about 5 times greater than the external field for periods shorter than a minute. The enhancement decreases versus period and the induced field is not more than 10% of the

external field for $T \geqslant 2$ hours. Note that in the Earth the induction is significant even for periods as great as some years.

On the right of Figure 6 the apparent resistivity curve, which was calculated by the data of Figure 5, is compared with the typical apparent resistivity for stable zones of the Earth. Evidently, the lunar resistivity is much greater than the Earth's. Its values obtained by Niblett transformation are compared on the left of Figure 6 with corresponding data for the stable zones of the Earth. The highest resistivity ($> 10^5$ Ωm) is observed in the uppermost part of the lunar mantle with thickness about 100–150 km. At the base of this high-resistivity layer the resistivity decreases sharply to 10^3 Ωm (Dyal *et al.*, 1976). At greater depths the decrease is more gradual.

Note that non-uniqueness of the inverse problem allows conductivity models with a spike between 150 and 200 km (Sonett and Colburn, 1967; Egorov, 1978).

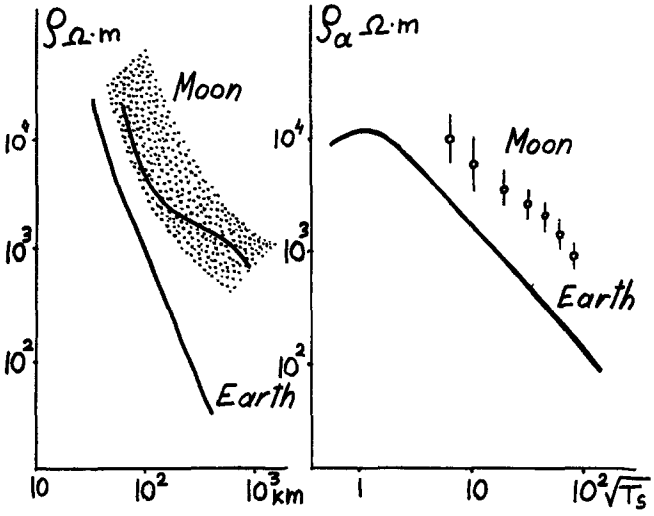

Fig. 6. Comparison of the apparent and true resistivities for the results obtained by Dyal *et al.* (1976).

Some Selenological Conclusions

The main conclusion is the absence of significant partial melting at depths less than 600 or 700 km. It is known that only 5% of basalt melt decreases the mantle resistivity to some tens of ohm m. The high values of lunar mantle resistivity suggest that the thickness of the solid lithosphere is at least 600 or 700 km, i.e. nearly half the lunar radii.

Many authors have attempted to estimate the temperature distribution inside the Moon using the laboratory dependence of resistivity on temperature.

One can attempt to translate the geotherm for the Earth's stable zones into the selenotherm by the simple comparison of the lunar and Earth's depths with the same resistivity. Results are shown in Figure 7; however their validity depends strongly on the similarity of the geochemistry, heat source distribution, etc.

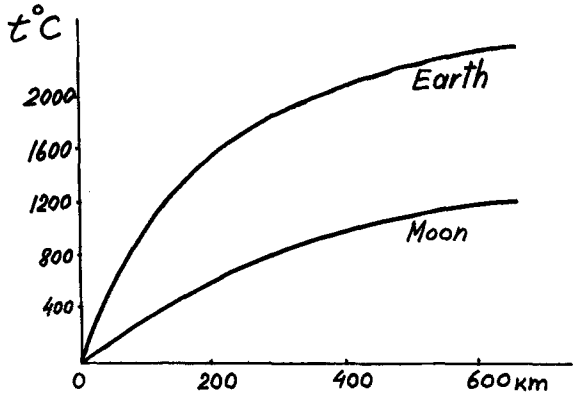

Fig. 7. Comparative Moon and Earth temperature profiles.

Regional Anomalies of Lunar Conductivity

It is supposed that the lunar conductivity model obtained by Apollo 12 data and supported by Apollo 16 measurements has a global scale. However, the observations made by Apollo 15 near the southeastern boundary of Mare Imbrium and the southwestern boundary of Mare Serenitatis show a strong signal anisotropy (Schubert *et al.*, 1974). Since there is no near-surface conductivity on the Moon, this anisotropy could be due to a deep lateral inhomogeneity. A similar tendency towards linear polarization was discovered at the eastern boundary of Mare Serenitatis by analyses of magnetic fluctuations in the period band 5–150 sec simultaneously observed by Lunokhod 2 and Apollo 16 (Figure 8) during January–March of 1973 (Vanyan *et al.*, 1979).

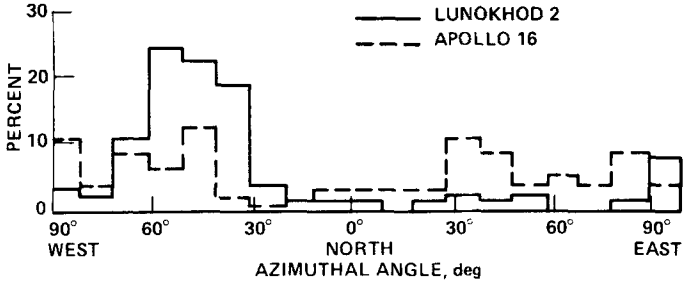

Fig. 8. Azimuthal distribution of horizontal magnetic variations. The solid line represents Lunokhod 2 data and the dashed line represents Apollo 16 data. The percentage of intervals in which the fluctuations were predominantly within a given azimuthal direction is plotted as a function of the azimuthal angle measured from north.

These are two mathematical models to explain the observed anisotropy. The two-current model (Figure 9(b)) consists of a deep layer overlain by an upper current layer

with a hole (Schubert and Schwartz, 1975). In the second model (Figure 9(a)) a perfect conductor is proposed at the base of the uppermost high-resistivity lunar shell. Beneath Mare Imbrium and Mare Serenitatis the depth of the conductor increases. For both models the magnetic force lines are drawn into the high-resistive area beneath the Mare. An edge effect appears causing signal anisotropy. The situation is quite similar to the telluric field behaviour near a depression filled by conductive sediments (Figure 9(c)). In Figure 10(b)) an example is presented in which the telluric vectors look toward the high-conductive southern part of the Caspian Sea.

For a thin dielectric shell of thickness d we can use the height integrated horizontal magnetic induction:

$$\beta = \int_0^d \boldsymbol{B}\, \mathrm{d}z \approx d.\boldsymbol{B}.$$

Continuity of $\boldsymbol{B}$ yields the equation for the two-dimensional divergence: $\mathrm{Div}.\,\beta = \mathrm{B}_{r0} - \mathrm{B}_{rd}$, where indexes 0 and d indicate the upper and lower boundaries of the dielectric shell.

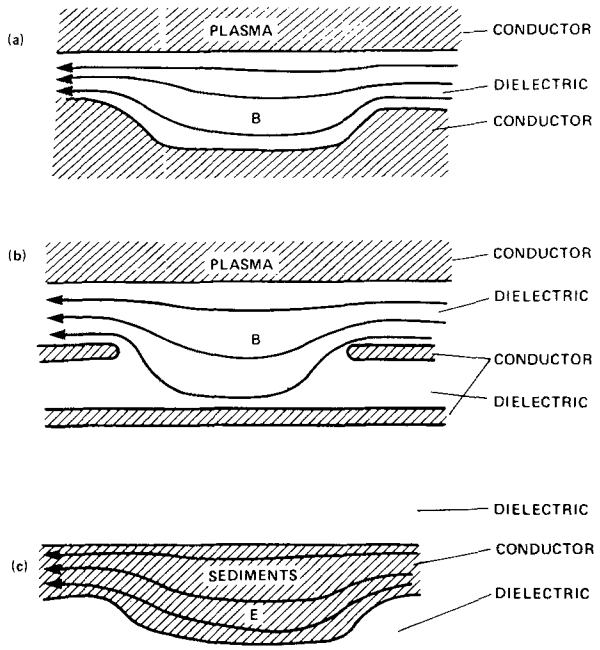

Fig. 9. Types of conductivity anomaly models. Electrically conducting material is shaded while dielectric material is not. The magnetic and electric fields are denoted by $\boldsymbol{B}$ and E, respectively. (a) The area under Serinitatis is modelled by a thickening of a dielectric layer between the highly conducting solar plasma above and lunar mantle below. (b) Model used by Schubert *et al.* (1974) in which a current sheet with a hole lies between the solar plasma above and a current layer below. (c) A terrestrial conductivity anomaly in which highly conducting sediments lie between the lower conducting atmosphere and crust.

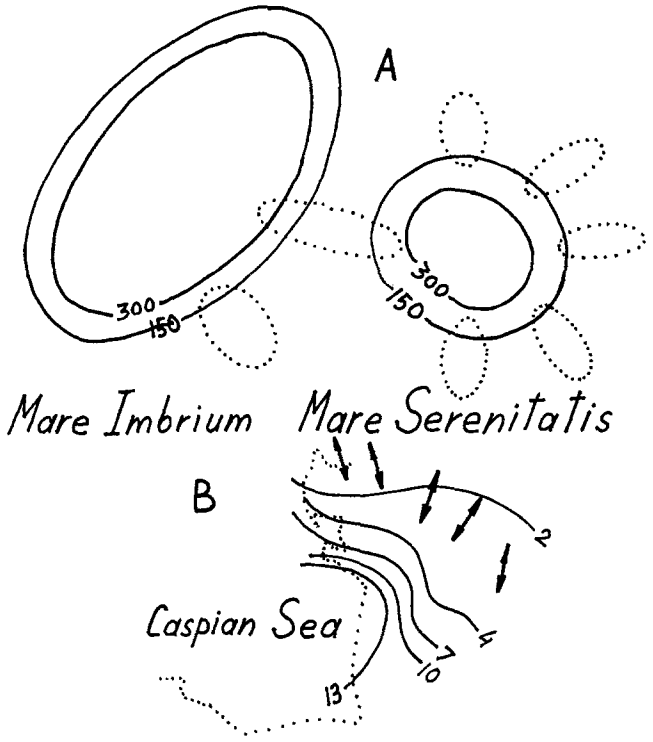

Fig. 10. (a) Calculated lunar magnetic ellipses (dotted lines). Isolines indicate the thickness of the uppermost dielectric layer (in km). (b) Experimental directions of main axis of the telluric ellipses (arrows). Isolines indicate the total conductivity of sediments in 10^3 mho at the southern part of the Caspian Sea.

If one assumes the inner part of the Moon to be a good conductor, then $B_{rd} = 0$, and we obtain:

$$d \operatorname{Div} \boldsymbol{B} + (\boldsymbol{B} \cdot \operatorname{grad} d) = B_{r0} \,. \tag{5}$$

Equation (5) was solved by a finite-difference method for the model with d = 150 km everywhere except Mare Imbrium and Mare Serenitatis, where d = 300 km. In Figure 10(a) the results of numerical modelling are shown to demonstrate the directions of axes of the magnetic ellipses at some points around Mare Serenitatis and Mare Imbrium. The primary field was assumed to be circularly polarized (Vanyan *et al.*, 1979).

References

Dyal, P., Parkin, C.W., and Daily, W.D.: 1974, Soviet-American Conference on Cosmochemistry of the Moon and Planets.

Dyal, P., Parkin, C.W., and Daily, W.D.: 1976, Third Workshop on Electromagnetic Induction in the Earth and Moon.

Egorov, I.V.: 1978, 'Peculiarities of the EM-induction in the Moon', Geomagnetic Research N22 (in Russian).

Schubert, G., and Schwartz, K.: 1975, *Phys. Earth Planet. Int.* **10**, 55.

Schubert, G., Schwartz, K., Sonett, C.P., Colburn, D.S., and Smith, B.F.: 1973, Proc. Fourth Lunar Science Conference.

Schubert, G., Smith, B.F., Sonett, C.P., Colburn, D.S., and Schwartz, K.: 1974, *Science* **183**, 1195.

Schwartz, K., and Schubert, G.: 1973, *J. Geophys. Res.*

Sonett, C.P., and Colburn, D.S.: 1967, *Nature* **216**, 340-343.

Sonett, C.P. *et al.*: 1972, *Geochim. Cosmochim. Acta.,* Suppl. 3, 2309.

Vanyan, L.L., and Egorov, I.V.: 1973, Cosmic Res. N6 (in Russian).

Vanyan, L.L., Vnuchkova, T.A., Eronshenko, E.A., Fainberg, E.B., Dyal, P., Parkin, C.W., and Daily, W.D.: 1977, *The Moon* **17**, 259-262.

Vanyan, L.L., Vnuchkova, T.A., Egorov, I.V., Basilevsky, A.T., Eroshenko, E.G., Fainberg, E.B., Dyal, P., and Daily, W.D.: 1979, *The Moon and the Planets* **21**, 185-192.